

focused by a graded index (GRIN) lens and was directed perpendicular to the catheter axis by a microprism (Fig. 1, B and C). The distal optics were encased in a transparent housing. The beam was scanned circumferentially at four revolutions per second by rotation of the cable, fiber, and optical assembly inside the static housing. The catheter-endoscope was redesigned from an original prototype (17) to decrease its diameter, increase imaging speed, and reduce parasitic internal reflections. The confocal parameter of the distal lens was 1.9 mm, which corresponded to a focused beam diameter of 40  $\mu\text{m}$ . Power loss caused by suboptimal coupling and internal reflection within the catheter was 3 to 4 dB. The overall SNR of the OCT system with the catheter-endoscope was  $\sim 106$  dB. The catheter-endoscope had a diameter of 1 mm, which is small enough to allow imaging in a human coronary artery or access through the flush port of a standard endoscope.

OCT images of the *in vivo* rabbit esophagus allowed visualization of all layers of the esophageal wall (Fig. 2, A and B). For example, the innermost layer, the mucosa, was readily distinguished owing to its low reflectivity compared with the submucosa. Vascular structures were also identified within the wall (Fig. 2B). These high-resolution images demonstrate the capability of OCT to both resolve microstructural detail and image the entire rabbit esophagus to the serosa. *In vivo* OCT images of the rabbit trachea permitted differentiation of the pseudostratified epithelium, mucosa, and surrounding hyaline cartilage (Fig. 3A). Because most neoplasms of both the esophagus and respiratory tract originate in the epithelium, the ability of OCT to precisely identify the mucosa could have important clinical implications.

A technology capable of performing optical biopsy should prove to be a powerful diagnostic modality in clinical medicine. Optical biopsy is defined here as imaging tissue microstructure at or near the level of histopathology without the need for tissue excision. At least three clinical scenarios exist in which optical biopsy will likely have a considerable impact on patient management. The first is in situations in which sampling errors severely restrict the effectiveness of excisional biopsy, such as the high failure rates associated with blind biopsies used to screen the premalignant conditions of ulcerative colitis or Barrett's esophagus (18). A need also exists for optical biopsy when conventional excisional biopsy is potentially hazardous. Examples of vulnerable regions include the central nervous

system, the vascular system, and articular cartilage. Finally, the ability to image at the cellular level could improve the effectiveness of many surgical and microsurgical procedures including coronary atherectomy, transurethral prostatectomies, and microvascular repair (8, 19, 20).

#### REFERENCES AND NOTES

1. D. Huang *et al.*, *Science* **254**, 1178 (1991).
2. A. F. Fercher, C. K. Hitzinger, W. Drexler, G. Kamp, H. Sattmann, *Am. J. Ophthalmol.* **116**, 113 (1993).
3. E. A. Swanson *et al.*, *Opt. Lett.* **18**, 1864 (1993).
4. M. R. Hee *et al.*, *Arch. Ophthalmol.* **113**, 325 (1995).
5. C. A. Puliafito *et al.*, *Ophthalmology* **102**, 217 (1995).
6. J. G. Fujimoto *et al.*, *Nature Med.* **1**, 970 (1995).
7. J. M. Schmitt, A. Knüttel, M. Yadlowsky, M. A. Eckhaus, *Phys. Med. Biol.* **39**, 1705 (1994).
8. M. E. Brezinski *et al.*, *Circulation* **93**, 1206 (1996).
9. J. M. Schmitt, M. J. Yadlowsky, R. F. Bonner, *Dermatology* **191**, 93 (1995).
10. G. J. Tearney *et al.*, *Am. J. Gastroenterol.*, in press.
11. B. E. Bouma, G. J. Tearney, I. P. Bilinsky, B. Golubovic, J. G. Fujimoto, *Opt. Lett.* **21**, 1839 (1996).
12. A. Seas, V. Petricevic, R. R. Alfano, *ibid.* **17**, 937 (1992).
13. V. M. Gelikonov *et al.*, *JETP Lett.* **61**, 149 (1995).
14. G. J. Tearney *et al.*, *Opt. Lett.* **21**, 1408 (1996).
15. K. F. Kwong, D. Yankelevich, K. C. Chu, J. P. Heritage, A. Dienes, *ibid.* **18**, 558 (1993).
16. J. P. Heritage, A. M. Weiner, R. N. Thurston, *ibid.* **10**, 609 (1985).
17. G. J. Tearney *et al.*, *ibid.* **21**, 543 (1996).
18. R. W. Phillips and R. K. H. Wong, *Gastroenterol. Clin. N. Am.* **20**, 791 (1991).
19. G. J. Tearney *et al.*, *J. Urol.* **157**, 1913 (1997).
20. M. E. Brezinski *et al.*, *J. Surg. Res.*, in press.
21. The axial dimension of each OCT image was 2.3

mm, which was digitized to 248 pixels. Imaging could be performed with either 256 or 512 lateral pixels, corresponding to image acquisition times of 125 or 250 ms, respectively. All images were obtained with 512-pixel lateral resolution at four frames per second to optimize lateral sampling. The two-dimensional image data were displayed with a polar coordinate transformation and inverse gray scale. Data were recorded in both Super VHS and digital format.

22. *In vivo* imaging was performed on normal New Zealand White rabbits at 12 weeks of age. After the animals were anesthetized, the OCT imaging catheter-endoscope was introduced through a 2.3-mm guiding catheter into the gastrointestinal and respiratory tract. The respiratory tract was accessed directly through the trachea via a midline incision, and the gastrointestinal tract was entered through the oropharynx. Sites imaged included the oropharynx, esophagus, trachea, and bronchi (main, secondary, and tertiary). After imaging, the animals were killed and the imaged regions were excised and immersed in 10% formalin for routine histologic processing. The specimens were blocked in paraffin, cut into 5- $\mu\text{m}$  sections, and stained with hematoxylin and eosin (H&E) for microscopic examination.
23. The contributions of E. A. Swanson (MIT Lincoln Laboratory) are greatly appreciated. We thank J. Gamba and J. Taralli for technical support and C. Kopf for help with preparation of the manuscript. Supported in part by NIH contract NIH-9-RO1-EY11289-10 (J.G.F.), the Medical Free Electron Laser Program, Office of Naval Research contract N00014-94-1-0717 (J.G.F.), the Air Force Office of Scientific Research contract F49620-95-1-0221 (J.G.F.), the Joint Services Electronics Program contract DAAH04-95-1-0038 (J.G.F.), the Whittaker Foundation contract 96-0205 (M.E.B.), and NIH contract NIH-1-R29-HL55686-01A1 (M.E.B.).

16 January 1997; accepted 10 April 1997

## Exchange of Protein Molecules Through Connections Between Higher Plant Plastids

Rainer H. Köhler, Jun Cao, Warren R. Zipfel, Watt W. Webb, Maureen R. Hanson\*

Individual plastids of vascular plants have generally been considered to be discrete autonomous entities that do not directly communicate with each other. However, in transgenic plants in which the plastid stroma was labeled with green fluorescent protein (GFP), thin tubular projections emanated from individual plastids and sometimes connected to other plastids. Flow of GFP between interconnected plastids could be observed when a single plastid or an interconnecting plastid tubule was photobleached and the loss of green fluorescence by both plastids was seen. These tubules allow the exchange of molecules within an interplastid communication system, which may facilitate the coordination of plastid activities.

Plastids are plant cell organelles that perform metabolic and biosynthetic reactions, including carbon fixation and synthesis of

fatty acids, carotenes, purines, and pyrimidines. Plastids contain multiple copies of a genome that encodes a subset of the organelle's RNA and protein molecules (1). Nuclear-encoded proteins are synthesized in the cytosol as precursors with transit peptides that target them to and across the chloroplast double-membrane envelope (2). Plastids are generally regarded as autonomous organelles that multiply by division and sort into daughter cells (1). We have

R. H. Köhler, J. Cao, M. R. Hanson, Section of Genetics and Development, Cornell University, Biotechnology Building, Ithaca, NY 14853-2703, USA.  
W. R. Zipfel and W. W. Webb, School of Applied and Engineering Physics, Cornell University, Ithaca, NY 14853-2703, USA.

\*To whom correspondence should be addressed. E-mail: mrh5@cornell.edu

made some observations that indicate that vascular plant plastids are less independent than previously thought.

We targeted a modified GFP (3, 4) to plastids of tobacco and petunia plants (5)

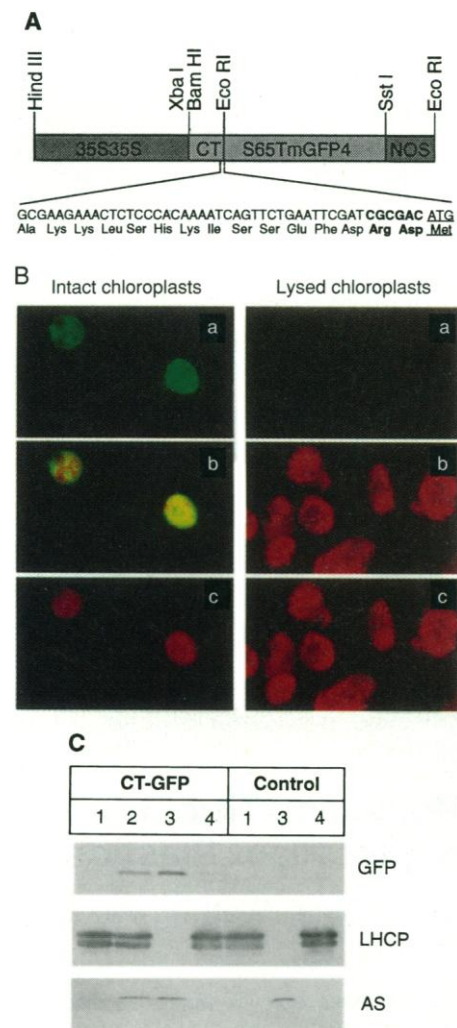


**Fig. 1. (A)** Chimeric gene construct (4) used to target GFP to plastids. 35S35S, double 35S promoter; CT, *recA* transit peptide; S65TmGFP4, GFP modified coding region; NOS, nopaline synthetase terminator region. After being processed by the transit peptidase, 15 amino acids derived from mature *recA* (regular type) and the adaptor sequence (bold type) are predicted to constitute the NH<sub>2</sub>-terminal portion of the transgenic GFP. **(B)** Purified chloroplasts from a transgenic plant, imaged by CLSM (7). (a) Green channel, (b) merged image, and (c) red channel. **(C)** Chloroplast fractionation to determine the location of GFP. An immunoblot of protein fractions of an untransformed control plant (control) and of a transgenic plant (CT-GFP), probed with antibodies reacting with three different proteins, is shown. Lane 1 shows 50  $\mu$ g of protein from a crude chloroplast fraction. Lane 2 shows 20  $\mu$ g of protein from purified chloroplasts. Lane 3 shows 20  $\mu$ g of soluble proteins from purified chloroplasts. Lane 4 shows 20  $\mu$ g of insoluble membrane fraction of purified chloroplasts.

by expression of a chimeric nuclear gene (4) in which the GFP coding region was connected to the transit peptide from the *Arabidopsis* chloroplast *recA* gene (Fig. 1A). The *recA* transit sequence resulted in the targeting of GFP to the stroma, the aqueous matrix of the plastid. When leaf cells were disrupted and chloroplasts were separated on a Percoll gradient (6) and examined by confocal laser scanning microscopy (CLSM) (7), intact chloroplasts exhibited the green fluorescence characteristic of GFP and the red autofluorescence of chlorophyll (Fig. 1B). Purified chloroplasts were disrupted by hypo-osmotic shock and separated into membrane and soluble portions (8). The broken chloroplast membrane fraction, which contains envelope and thylakoid membranes as well as intact thylakoids, still exhibited red (chlorophyll) fluorescence but had lost all GFP fluorescence (Fig. 1B). In immunoblots (Fig. 1C), the GFP signal was located primarily in the soluble fraction, as was anthranilate synthase (AS), a stromal enzyme (9). The

membrane fraction contained the light-harvesting chlorophyll *a/b* protein (LHCP) (10) and a very weak GFP signal that probably resulted from contamination of the membrane fraction with stromal proteins. In cells of transgenic plants, GFP fluorescence was only visible within chloroplasts [(11) and Fig. 2].

Thin green tubules emanating from chloroplasts are visible in leaf tissue in the transgenic plants when the tissue is examined with a standard epifluorescence microscope or by CLSM [(11) and Fig. 2]. Tubules are visible in all tissues studied so far but vary in abundance within a given cell type and between different tissue types. In some cells, tubules are evident on most chloroplasts, but in the majority of leaf cells, only a few or no tubules are visible. The tubular projections arise initially as protuberances from the chloroplast surface that elongate and extend (Fig. 3). They are dynamic in the living cell, continuously changing their shape, moving around, shrinking back, and sometimes connecting

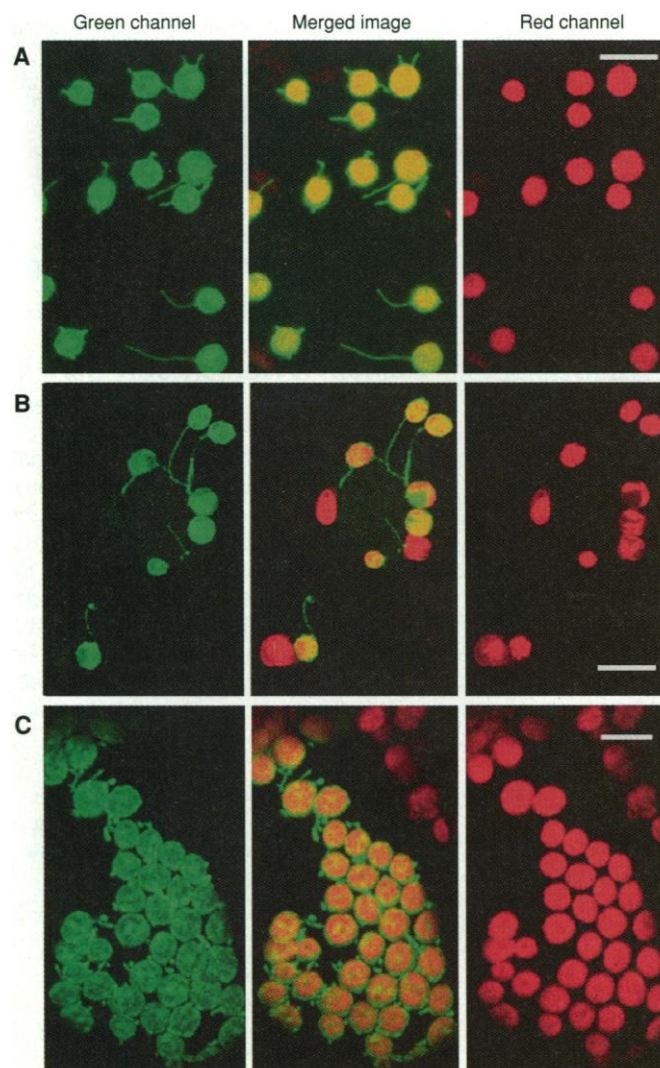


**Fig. 2.** Tubules and tubular interconnections between chloroplasts of transgenic plants, imaged by CLSM. **(A)** Petunia epidermal cell. Projection of 24 optical sections taken at 0.1- $\mu$ m intervals along the optical axis. **(B)** Tobacco trichome cell. Projection of 15 optical sections taken at 0.2- $\mu$ m intervals. **(C)** Tobacco mesophyll cell. Projection of 36 optical sections taken 0.2  $\mu$ m apart. Scale bars, 10  $\mu$ m.

with other chloroplasts. The tubules do not contain chlorophyll that is detectable by autofluorescence. Their width appears to range from 0.35 to 0.85  $\mu\text{m}$ , and they may be as long as 15  $\mu\text{m}$  [Fig. 2 and (11)]. Sometimes a plastid protuberance extends and appears to encircle a nonfluorescent body; this is similar to a finger curled around a sphere.

To determine whether exchange of protein occurs through plastid interconnections, we used a two-photon laser scanning microscope (12) to selectively photobleach individual plastids or individual interconnecting tubules in living plant cells (Fig. 4). When the laser was targeted to an individual plastid, loss of the GFP signal was restricted to this individual plastid, and the plastid remained photobleached after irradiation ceased during the following 35 s of observation (Fig. 4A). The synthesis and import of GFP from the cytoplasm are not sufficiently rapid to restore fluorescence over this time period. After the irradiation, nearby plastids that were not connected to the irradiated plastid remained brightly fluorescent (Fig. 4A). When the laser beam was targeted to an interconnecting chloroplast tubule (Fig. 4B), both interconnected plastids exhibited some photobleaching after 2.5 s of irradiation. A further 2.5 s of irradiation resulted in further loss of GFP fluorescence in both plastids (Fig. 4B). This indicates a rapid flow of GFP through the tubular interconnection between the plastids. We also revealed the flow of GFP from one plastid to another by photobleaching one of two interconnected plastids (Fig. 4, C and D). A 2-s irradiation reduced the GFP fluorescence in the irradiated plastid to  $\sim 30\%$  of the initial value. During the next 7 s, GFP fluorescence in the irradiated plastid partially recovered to 53% of the initial value; simultaneously, GFP fluores-

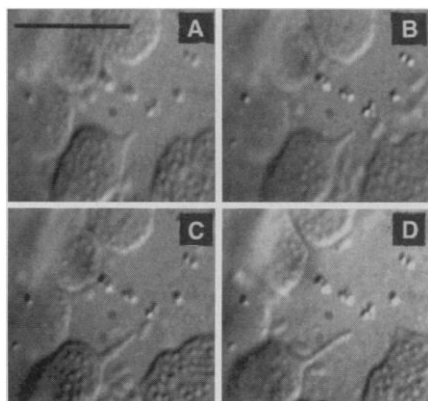


**Fig. 3.** Tubule in a wild-type plant cell (18). (A through D) Tubule extending from the chloroplast surface in a living spinach mesophyll cell. Images were taken at about 30-s intervals. Scale bar, 10  $\mu\text{m}$ .

cence in the connected plastid decreased to  $\sim 60\%$  of its initial value, which indicates flow and equilibration of unbleached GFP between the nonirradiated plastid and the bleached plastid.

Tubules emanating from the chloroplast are also observable in nontransgenic wild-type spinach and tobacco [Fig. 3 and (11)] and have been described in a variety of other wild-type vascular plant species (13, 14). Light microscopic studies and a movie made by Wildman and his colleagues (13) show dynamic protuberances extending from leaf chloroplasts of tobacco and spinach that sometimes connect to other chloroplasts. Protuberances emanating from chloroplasts have also been imaged in different species by electron microscopy (14). Because interpretation of these structures was difficult, their existence has not been widely known or accepted.

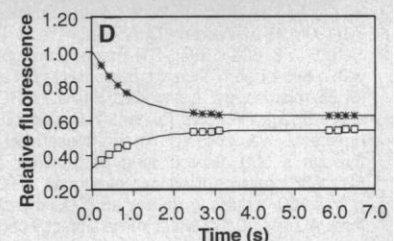
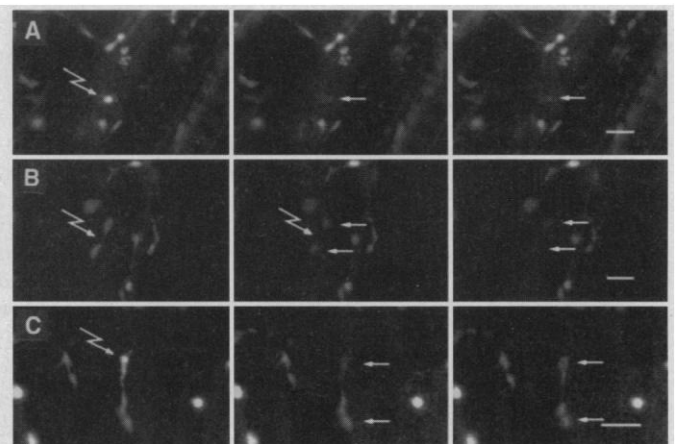
Interconnections between chloroplasts have also been detected in *Euglena* and *Acetabularia* (15, 16), although chloroplasts in these unicellular organisms differ from those of vascular plants (1). In *Acetabularia*, chloroplast tubules that sometimes extend over hundreds of micrometers between chloroplasts are common (15); except for their length, these tubules

appear quite similar to the tubules we describe in higher plants. In *Euglena*, tubules connecting chloroplasts appear at specific times of the cell cycle, shortly before chloroplast division (16). Cell cycle stage-specificity of chloroplast tubules in tobacco and petunia was not investigated in our experiments, but obvious differences exist in the abundance of tubular projections in individual cells of the same tissue.

Chloroplasts are thought to have arisen from cyanobacterial endosymbionts (1, 17). The tubular connections that we observed are reminiscent of bacterial pili. Further analysis may reveal whether the tubules have any functional or compositional similarity to structures that allow the exchange of macromolecules between bacteria.

A number of functions can be envisioned for the stroma-containing interconnecting tubules. They may allow plastids to share molecules such as metabolic intermediates, nucleic acids, enzymes, and regulatory proteins. In *Acetabularia*, it has been proposed that the tubules support chloroplast motility (17). In vascular plants, the tubules may permit the plastid to sample volumes of the cell in which concentrations of useful molecules are higher than in the

**Fig. 4.** Localized two-photon photobleaching (12) of GFP in tobacco root plastids. Jagged arrows indicate regions that will undergo localized photobleaching. Straight arrows indicate plastids after photobleaching. Scale bars, 5  $\mu\text{m}$ . (A) Control photobleaching of an unconnected plastid. (Left) The plastid at the jagged arrow in the left panel was photobleached for 2 s with an 800-nm pulsed excitation (100 fs pulse width). (Middle) The plastid immediately after bleaching ( $\sim 0.5$  s). (Right) The plastid 35 s after bleaching. (B) Depletion of GFP by localized photobleaching of a connecting tubule. (Left) A 5- $\mu\text{m}$  line (800 nm, 100 fs) was scanned across the interconnection at the jagged arrow for 2.5 s. (Middle) The image acquired after the first photobleaching shows the depletion of GFP in both connected plastids. (Right) Image acquired after an additional 2.5-s line scan of connecting tubule, which shows a further depletion of GFP fluorescence. (C) Photobleaching of GFP fluorescence of one plastid of a connected plastid pair. (Left) Prebleach image; a 5- $\mu\text{m}$  line was scanned across the plastid at jagged arrow for 2.5 s. (Middle) The image 0.6 s after bleaching. (Right) The image 6 s after bleaching; the signal in the bleached plastid has partially recovered, whereas the signal in the connected plastid has decreased. (D) Fluorescence recovery curve from the image time series shown in (C). Four images were acquired at 0.210-s intervals, separated by a 2.2-s pause, for a total of 12 images. The plot shows the mean value from a 30 by 60 pixel box around the bleached plastid ( $\square$ ), the connected unbleached plastid ( $\ast$ ) normalized to the prebleach image values [left panel in (C)], and the concurrent changes in the signal in the coupled plastids relative to their initial value.



region next to the plastid body, especially if the tubules encircle other organelles such as mitochondria.

## REFERENCES AND NOTES

1. Reviewed in J. K. Hooper, *Chloroplasts* (Plenum, New York, 1984), and J. T. O. Kirk and R. A. E. Tilney-Bassett, *The Plastids: Their Chemistry, Structure, Growth and Inheritance* (Elsevier/North-Holland, Amsterdam, ed. 2, 1978).
2. Reviewed in R. Cline and R. Henry, *Annu. Rev. Cell Dev. Biol.* **12**, 1 (1996).
3. R. H. Köhler, W. R. Zipfel, W. W. Webb, M. R. Hanson, *Plant J.* **11**, 613 (1997).
4. The modified GFP4 coding region [J. Haseloff and B. Amos, *Trends Genet.* **11**, 328 (1995)], which was further altered (3) by a Ser-to-Thr mutation at codon 65 (S65T:mGFP4), was fused in frame with the *Arabidopsis* recA transit peptide (CT) [H. Cerutti, M. Osman, P. Grandoni, A. T. Jagendorf, *Proc. Natl. Acad. Sci. U.S.A.* **89**, 8068 (1992)].
5. The CT-GFP fusion was cloned into the Bam HI and Sst I sites of pBIN19-based binary vector pCT37 [C. M. Tobias and J. B. Nasrallah, *Plant J.* **10**, 523 (1996)], introduced into *A. tumefaciens* pCIB542/A136 [E. E. Hood, G. L. Helmer, R. T. Fraley, M. D. Chilton, *J. Bacteriol.* **168**, 1291 (1986)], and used to transform plants [R. B. Horsch *et al.*, *Science* **227**, 1229 (1985)].
6. We prepared the chloroplasts by breaking tobacco leaf cells with a mortar and pestle, followed by differential centrifugation and separation on a Percoll gradient according to J. Huang, E. Hack, R. W. Thornburg, and A. M. Meyer [*Plant Cell* **2**, 1249 (1990)], except that a 15%/40%/80% Percoll gradient was used.
7. A BioRad MRC-600 CLSM with a standard K1/K2 filter set was used. Pseudocolor similar to the color observed by eye with the Olympus microscope was added to the images by the import of data collected in the green and red channels from the BioRad microscope into Adobe Photoshop. Optical sections were taken along the optical axis and projected into one image with the COMOS software (BioRad).
8. Purified chloroplasts were lysed for 10 min at 4°C in 50 mM Hepes at pH 7.5 and 1 mM phenylmethylsulfonyl fluoride and separated by 15 min of centrifugation at 4°C into a soluble and a membrane fraction. The membrane fraction was washed twice in lysis buffer. Protein was quantified by the Bradford protein assay (Bio-Rad) and separated by SDS-polyacrylamide gel electrophoresis on a 12% gel, transferred to nitrocellulose, and probed with 1:1000 dilutions of the different antibodies as described in (3).
9. J. Zhao and R. L. Last, *J. Biol. Chem.* **270**, 6081 (1995).
10. L. A. Payan and K. Cline, *J. Cell Biol.* **112**, 603 (1991).
11. R. H. Köhler, J. Cao, W. R. Zipfel, W. W. Webb, M. R. Hanson, data not shown.
12. W. Denk, J. H. Strickler, W. W. Webb, *Science* **248**, 73 (1990); R. M. Williams, D. W. Piston, W. W. Webb, *FASEB J.* **8**, 804 (1994). The images were obtained with a two-photon microscope consisting of a Zeiss IM-35 microscope, a modified BioRad MRC-600, and a Spectra-Physics Tsunami Ti:S laser. GFP fluorescence was collected in non-descanned mode through a 500 dichroic long pass mirror and a 520DF35 emission filter; excitation was at 800 nm (with a 100-fs pulse width and an 80-MHz repetition rate). A Zeiss 40/1.2 water immersion objective lens was used. Localized photobleaching was carried out by repetitive rapid line scanning of the targeted sub-cellular structure.
13. S. G. Wildman, T. Hongladarom, S. I. Honda, *Science* **138**, 434 (1962); S. G. Wildman, in *Biochemistry of Chloroplasts*, T. W. Goodwin, Ed. (Academic Press, New York, 1967), vol. 2, pp. 295–319; T. Hongladarom, I. Shigeru, S. I. Honda, S. G. Wildman, "Organelles in Living Plant Cells," color sound film produced by P. Kahana and Y. Kahana (Extension Media Center, University of California, Berkeley, 1965); D. Spencer and S. G. Wildman, *Aust. J. Biol. Sci.* **15**, 599 (1962).
14. M. Vesik, F. V. Mercer, J. V. Possingham, *Aust. J. Bot.* **13**, 161 (1965); T. E. Weier and W. W. Thomson, *Am. J. Bot.* **49**, 807 (1962).
15. D. Menzel, *Protoplasma* **179**, 166 (1994).
16. T. Osafune, T. Ehara, E. Hase, J. A. Schiff, *J. Electron Microsc.* **42**, 201 (1993); T. Ehara, T. Osafune, E. Hase, *Exp. Cell Res.* **190**, 104 (1990).
17. M. W. Gray, *Int. Rev. Cytol.* **141**, 233 (1992).
18. Differential interference contrast microscopic images were collected with an Olympus BX50 microscope equipped with a cooled charge-coupled device camera [Optronics (Chelmsford, MA) DEI-750T].
19. We thank J. Haseloff for the mGFP4 gene and T. Horiagon, R. Last, S. Lawrence, and K. Cline for antibodies to GFP, AS, and LHCP. Supported by DOE Energy Biosciences Program grant DE-FG02-89ER14030 to M.R.H. and grants to W.W.W. and Developmental Resources for Biophysical Imaging and Opto-electronics by NSF (DIR8800278) and NIH (RR04224 and R07179).

15 January 1997; accepted 9 May 1997

## Regulatory Phosphorylation of AMPA-Type Glutamate Receptors by CaM-KII During Long-Term Potentiation

Andres Barria, Dominique Muller, Victor Derkach, Leslie C. Griffith, Thomas R. Soderling\*

Long-term potentiation (LTP), a cellular model of learning and memory, requires calcium-dependent protein kinases. Induction of LTP increased the phosphorus-32 labeling of  $\alpha$ -amino-3-hydroxy-5-methyl-4-isoxazolepropionic acid (AMPA)-type glutamate receptors (AMPA-Rs), which mediate rapid excitatory synaptic transmission. This AMPA-R phosphorylation appeared to be catalyzed by  $\text{Ca}^{2+}$ - and calmodulin-dependent protein kinase II (CaM-KII): (i) it correlated with the activation and autophosphorylation of CaM-KII, (ii) it was blocked by the CaM-KII inhibitor KN-62, and (iii) its phosphorus-32 peptide map was the same as that of GluR1 coexpressed with activated CaM-KII in HEK-293 cells. This covalent modulation of AMPA-Rs in LTP provides a postsynaptic molecular mechanism for synaptic plasticity.

Long-term potentiation is a prolonged enhancement in synaptic efficacy that may underlie certain types of learning and memory, but its molecular mechanisms are unclear (1). Considerable evidence implicates changes in presynaptic transmitter release, postsynaptic responses, and synaptic structural changes. Postsynaptic elevations in  $\text{Ca}^{2+}$  and  $\text{Ca}^{2+}$ -dependent protein kinases are required for establishment of LTP, and a likely target of these kinases is AMPA-Rs (2) because (i) their responsiveness is enhanced after elevations of postsynaptic  $\text{Ca}^{2+}$  (3) or by LTP induction (4), and (ii) these changes are blocked by KN-62 (3, 5), a CaM-K inhibitor (6). Activated CaM-KII enhances AMPA-R responsiveness in CA1 neurons in hippocampal slices and many other systems (7–9). In the slices, expression or infusion of activated CaM-KII also increases synaptic current and occludes subsequent induction of LTP. However, a key observation, direct phosphorylation of AMPA-Rs in response to LTP, has

not been previously demonstrated.

Induction of LTP produces a small increase in the  $\text{Ca}^{2+}$ -independent or constitutive activity of CaM-KII (10). CaM-KII can autophosphorylate on multiple sites (2, 11), so to confirm that the constitutive CaM-KII activity was due to autophosphorylation of Thr<sup>286</sup>, we used a phosphospecific antibody, Ab<sub>P-Thr<sup>286</sup></sub>. This antibody was specific for P-Thr<sup>286</sup> in CaM-KII, reacting with autophosphorylated wild-type CaM-KII but not with the autophosphorylated Thr<sup>286</sup>-Ala mutant (Fig. 1A). Protein immunoblot analyses with Ab<sub>P-Thr<sup>286</sup></sub> of a hippocampal slice extract detected multiple immunoreactive bands, but only the one corresponding to the 50-kD  $\alpha$ -CaM-KII was selectively blocked by preadsorption with the phosphopeptide antigen (Fig. 1B). Induction of LTP in the CA1 region of hippocampal slices with theta-burst stimulation (10) resulted in a small, stable increase in immunoreactivity to Ab<sub>P-Thr<sup>286</sup></sub> (Fig. 1C). The magnitude of the increase is in general agreement with the estimate that about 10% of synapses are potentiated by theta-burst stimulation (12). The enhanced phosphorylation of Thr<sup>286</sup> was not due to an LTP-mediated increase in CaM-KII protein, because immunoreactivity with a general CaM-KII antibody ( $n = 4$ ) did not increase at 5 min

A. Barria, V. Derkach, T. R. Soderling, Vollum Institute, Oregon Health Sciences University, Portland, OR 97201, USA.

D. Muller, Department of Neuropharmacology, Centre Medical Universitaire, 1211 Geneva 4, Switzerland.  
L. C. Griffith, Department of Biology, Brandeis University, Waltham, MA 02254, USA.

\*To whom correspondence should be addressed.